Mon. Not. R. Astron. Soc. **000**, 1–8 () Printed 29 August 2006 (MN LATEX style file v2.2)

Analysis and calibration of CaII triplet spectroscopy from low resolution VLT/FLAMES observations

Giuseppina Battaglia[1⋆], M.Irwin[2], E.Tolstoy[1], Amina Helmi[1], V.Hill[3] & **and others?**

[1] *Kapteyn Institute, P.O.Box 800, 9700 AV Groningen, The Netherlands*
[2] *Institute of Astronomy, Cambridge University, UK*
[3] *GEPI, Observatoire de Paris Meudon, France*

29 August 2006

ABSTRACT

We demonstrate that low resolution spectroscopic estimates of the overall metallicity of individual K-giants in dwarf spheroidal galaxies agrees to ±0.1dex with detailed high resolution spectroscopic analysis of the same stars over the range -2.5 < [Fe/H] < -0.5 .

.... we describe analysis method ....

Using a standard calibration based on gc sequences based on CaII triplet measurements at a resolution of R ≈ 6500

...... calibrated on standard globular cluster sequences

...... error analysis ....

...... velocities 1-2 km s^{-1}

.... EWs to 0.1 dex

Key words:

1 INTRODUCTION

....

The CaII triplet (CaT) method is routinely used to estimate overall [Fe/H] abundances from K-giants in nearby galaxies (*e.g.* Rutledge, Hesser & Stetson) and also provides an accurate radial velocity estimate. Both measurements are facilitated by the strength of the CaT lines in this part of the spectrum and by the red colours of the target stars. However, the most commonly used calibration of the CaT is based on measurements of handfuls of K-giants from a limited range of galactic globular clusters. Although the method is straightforward, it is not *apriori* obvious how well this calibration applies to stars in individual dwarf galaxies, which in general have a much more complex and extended star formation history compared to the cluster calibrators.

In this paper we describe the data reduction steps we use within the DART collaboration to estimate abundances and velocities from observations in the CaT region. We also discuss the verification of the overall calibration and accuracy of the velocity and abundance measurements: by comparison of results from independent CaT observations; cross-checks with measurements made from high resolution observations of the same stars; observations of globular cluster calibrators; and by comparing with theoretical expectations based on signal-to-noise, resolution and line profile properties.

2 OBSERVATIONS AND DATA REDUCTION

All the LR CaII triplet observations were made using VLT/FLAMES in Medusa mode. This allows the simultaneous allocation of up to 132 fibres, including sky fibres, over a 25' diameter field-of-view. We used the GIRAFFE low resolution grating (LR8), which covers the wavelength range from 8206Å – 9400Å, and gives a resolution of R≈6500. This setup was used as part of the DART programme to obtain spectra for several different fields in each of the Sculptor, Fornax and Sextans dwarf spheroidal (dSph) galaxies. Of particular interest here are the central fields in Sculptor and Fornax which were also observed with a similar VLT/FLAMES setup but at high resolution (HR) with R≈20000 using the H10 (5339Å – 5613Å), H13 (6120Å – 6397Å), and H14 (6307Å – 6618Å) gratings. The HR analysis of the Sculptor and Fornax observations is described in more detail in (Hill *et al.* ....) and (Letarte *et al.* ....) respectively, but we discuss the salient features in a later section.

The data were all initially reduced using the GIRBLDRS[1] pipeline provided by the FLAMES consor-

⋆ Corresponding author. E-mail:gbattagl@astro.rug.nl

[1] available at SourceForge, http://girbldrs.sourceforg.net/

tium (Geneva Observatory, Blecha *et al.* 2003). This package provided individual spectral extraction and accurate wavelength calibration, based on daytime calibration arc exposures. The accuracy of the latter therefore relies heavily on the (proven) stability of the spectrographs. At the time we started this project no sky subtraction was available within this pipeline which lead us to develop several further reduction stages for the LR analysis.

2.1 Sky subtraction and wavelength refinement

An example of a spectrum produced by the GIRBLDRS pipeline is shown in figure 1. The numerous skylines visible in this part of the spectrum not only serve as an independent check on the overall wavelength calibration, but also enable an update of the wavelength calibration of the individual spectra.

Since the CaT lines only occupy a limited part of the LR spectra we optimised the sky subtraction and wavelength refinement for the range 8400Å – 8750Å and used the same derived parameters for the remaining spectral regions.

We first combine all the sky spectra (typically 10–20 sky fibres were allocated) using k-sigma clipping to remove spurious features. The average sky spectrum is then split into continuum and sky line components using an iterative k-sigma clipped non-linear filter (a combination of median and boxcar). The average "sky-line" spectrum is used to define a sky-line template mask, essentially to isolate those regions of the sky spectrum with significant features and mask out the remainder.

Processing of individual object spectra then proceeds as follows:

i. each spectrum is filtered as before to split the spectra into a line and continuum component, but this time additionally masking out those regions affected by sky lines to help in defining the continuum;

ii. the object line spectrum, which includes sky lines, is then cross-correlated with the masked line component of the average sky spectrum, to provide an accurate differential wavelength update and (re)interpolated to be on the same wavelength system as the average sky spectrum;

iii. sky subtraction then involves finding the optimum scale factor and profile matching kernel that produces a minimum L1 norm (average absolute deviation) when comparing the masked sky-line and object-line spectra, and applying it to the line-only spectra;

iv. finally the object continuum is added back to the wavelength-updated object-line spectrum, the sky continuum is removed used the sky-line scaling factor and the sky-subtracted spectrum is saved for the next stage in the processing.

The sky subtraction process described above involves three key components all of which are crucial to achieve good results. Accurate wavelength registration is absolutely vital for good sky subtraction and is (ironically) facilitated by the presence of copious numbers of strong sky lines. These sky lines are unresolved at this resolution and at the signal-to-noise achieved (see later) readily enables sub-km s^{-1} precision in wavelength alignment. This also has the added advantage of ensuring that systematic offsets due to wavelength calibration for later derived velocites are negligible. As a final step in this process, all the average sky spectra from each FLAMES observation, are cross-correlated with a chosen reference sky spectrum and used to put all the observations on the same internal system.

The effects of combining the sky spectra to form an average sky and re-interpolating the object spectrum to this average wavelength system, almost invariably results in a slight mis-match between the spectral line profiles of the object and average sky spectra. This is circumvented by applying a Hanning smoothing kernel to each in turn and finding which combination of smoothed and un-smoothed gives the best results (as determined by the optimum scale factor). More sophisticated adaptive kernel matching (*e.g.* Alard & Lupton 2000) is probably unwarranted in this case.

The optimum scaling factor, which in this case is chosen to minimise the L1 norm rather than the commoner L2 norm to reduce sensitivity to non-Gaussian outliers, is derived using a simple grid search with progressively finer step size. As noted previously, a mask is used to isolate the relevant regions of the sky spectrum to match. By first removing the continuua from both sky and object, more emphasis is placed on minimising the impact of sky lines residuals. Of course, implicit in the sky correction is the reasonable assumption that the derived scale factor for both sky lines and sky continuum is the same.

2.2 Velocity and equivalent width estimation

The first stage of the process is to estimate the continuum in a similar manner to the previous stage. Each spectrum is split into a line-only, and smoothly varying continuum-only component, using an iterative k-sigma clipped non-linear filter. This time the region around each CaT line is masked out, prior to filtering, to prevent the continuum tracking the wings of strong CaT lines. The effective scale length of the filtering is set to around 15Å which, in conjunction with the masking and iterative clipping, is fine enough to follow continuum trends without being affected by the presence of strong lines. At the same time an estimate of the overall signal-to-noise in the continuum is made by measuring the median continuum level in the CaT region and by measuring the pixel-to-pixel noise covariance matrix in regions containing no lines. The latter is needed to correct the apparent random noise for the cumulative smoothing effects of spectral interpolation and resampling, which we find typically results in a factor of ≈2 overall random noise reduction.

After normalising by the computed continuum the velocity is estimated by cross-correlating each spectrum with a model function template. The template is constructed from a zero-level continuum with three Gaussian absorption lines located at the vacuum rest wavelengths of the CaT lines superimposed. The Gaussian line depths are scaled in the ratio 3:5:4 to reflect the different strengths of real CaT lines and all are set to have a full width at half maximum (FWHM) = 2.35Å . An example of a continuum fitting to a Sculptor dSph K-giant spectrum together with the computed cross-correlation function and Gaussian fit to the peak is shown in figure 2.

An accurate estimate of the position of the cross-correlation peak is made by fitting a Gaussian to a localised region around the peak. This velocity is then used to define the wavelength region around each CaT line to use for EW estimation. After some trial and error we settled on a re-

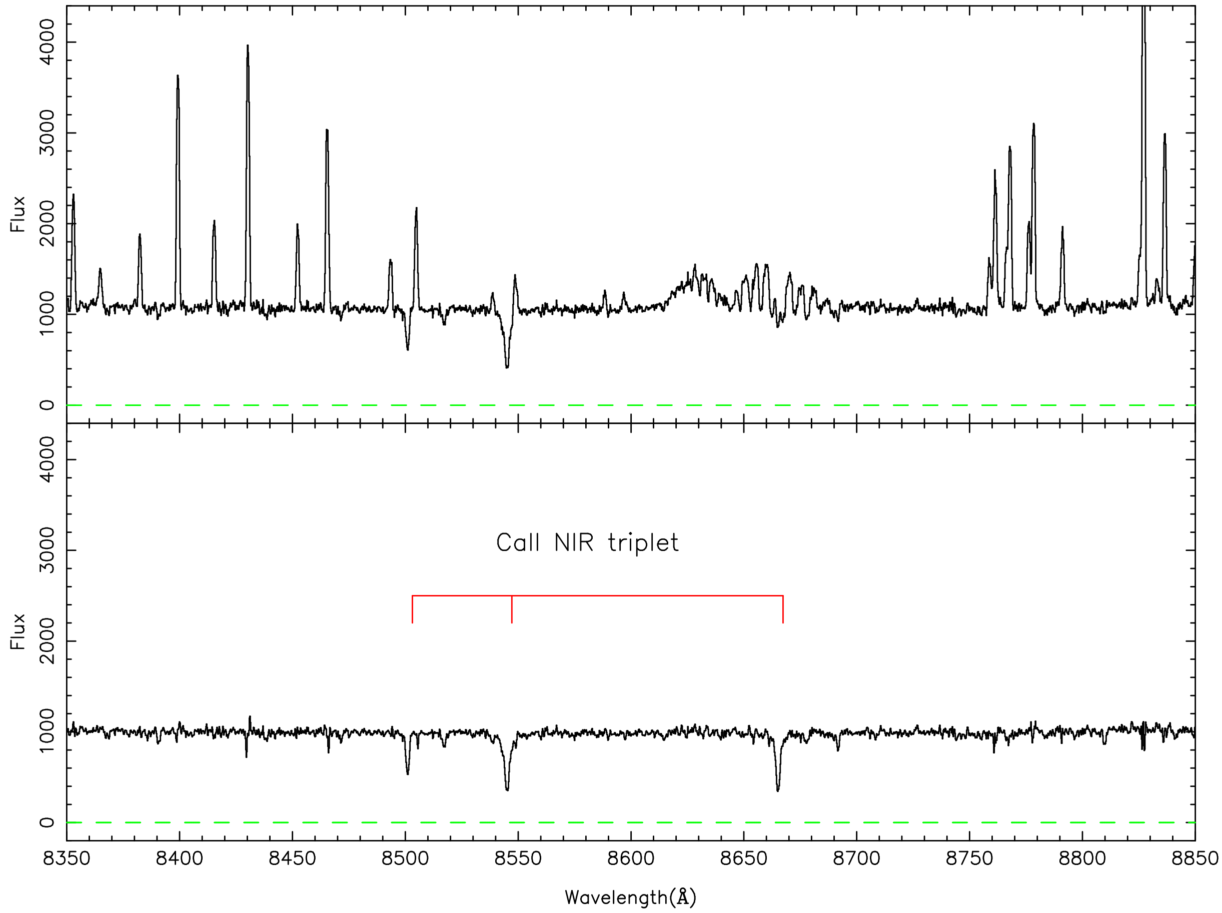

Figure 1. Example of automated LR sky subtraction from VLT/FLAMES data with CaT lines marked.

gion 15Å wide centred on each line as a reasonable tradeoff between including all the line flux and minimising the noise in the simple integral estimator. In addition to the straightforward sum we also fit individual unconstrained Gaussian functions to each CaT line over the same wavelength region and use the derived flux as an alternative EW estimator (see figure 2). This also allows a semi-independent check on the accuracy of the derived velocity by providing three separate velocity measures with associated errors. The weighted sum of these velocity errors provides the basic velocity error estimate for the velocity derived from the cross-correlation. We prefer to use the latter for the actual velocity estimate since it is effectively a constrained model fit. As a final step the derived velocity is corrected to a helio-centric system.

The combined equivalent widths for CaT lines #2 and #3 for both the integral and Gaussian fit are then compared and used to compute an overall correction to the Gaussian version. This is necessary since the real line profile is a complex function of many parameters, and in particular, the dampening wings visible in strong lines are distinctly non-Gaussian in appearance. This correction is equivalent to computing the average overlap integral between the real line profiles and the Gaussian fits and is accomplished by measuring the gradient between the two as a function of EW. We prefer to use the Gaussian-derived EW estimator since although the simple integral is unbiased it is also significantly noisier than a Gaussian fit. We show in the next section how the measurements of the continuum level and the random noise error in the continuum can be used to estimate errors in the EWs and velocities.

2.3 Error bounds for velocities and equivalent widths

For detailed abundance work most lines of interest are weak *e.g.* EW $\approx$ 100mÅ. A notable exception are the CaT lines used in the LR analysis which are generally heavily saturated and on the damped part of the curve-of-growth. Turbulence + rotation velocities of late-type giants typically only broaden the line profiles by $\approx$ a few km s^{-1}, hence the profile of the CaT lines, which are completely unresolved at R=6500, are dominated by intrinsic broadening due to saturation (typically FWHM 2Å – 3Å) and to a lesser extent by the convolution due to the resolution of the spectrograph (FWHM $\approx$1.3Å).

Despite the dampening wings, to first order the LR CaT lines can be reasonably well approximated by Gaussian functions (*e.g.* see figure 2) and we can use this to gain some insight into the limiting factors that determine the accuracy of the velocity and EW measurements.

Here we define resolution as FWHM = 2.35σ where σ is the Gaussian profile equivalent scale parameter. Since the

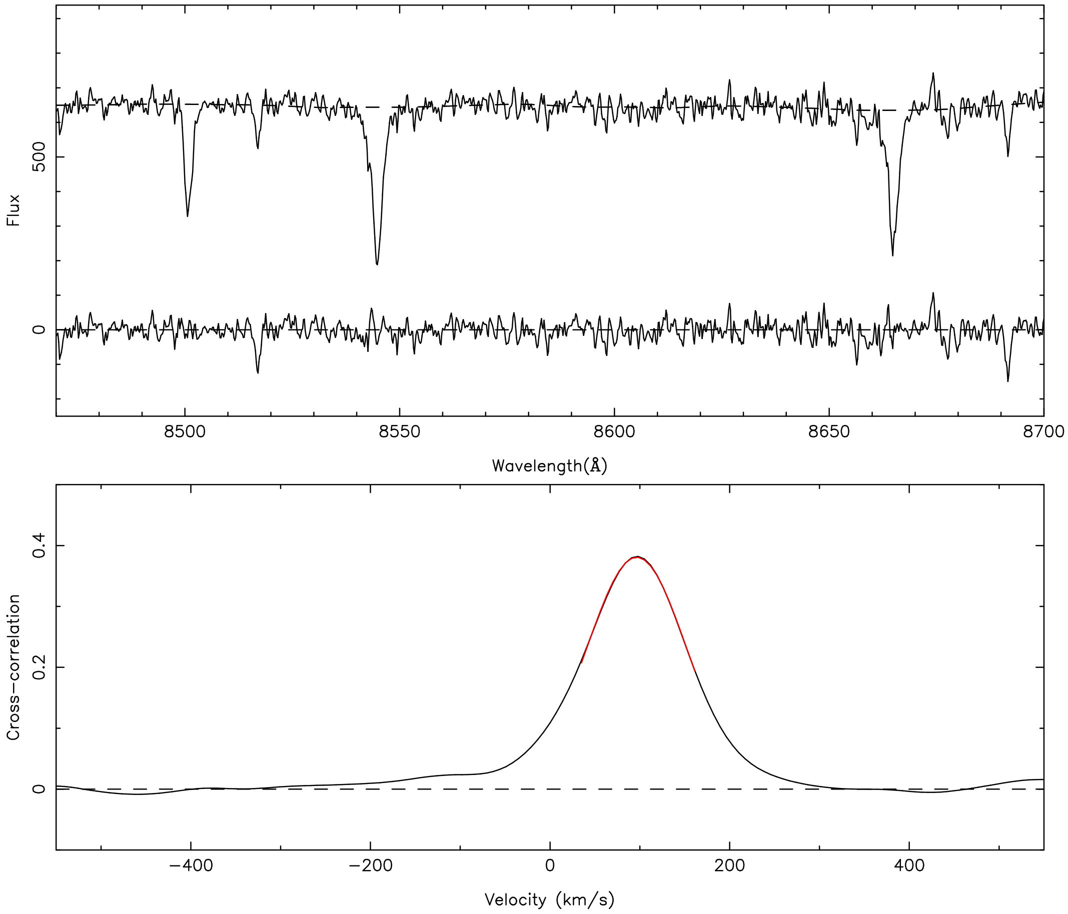

Figure 2. Upper panel: the upper plot shows the CaT region for a K-giant in the Sculptor dSph with derived [Fe/H] = -1.50 dex LR (-1.63 dex HR), showing an example of automated continuum fitting (dashed line); the lower plot shows the residual after continuum removal and after subtracting Gaussian model fits to the three CaT lines. Lower panel: the derived cross-correlation function and associated Gaussian fit around the peak region.

total line flux is then $I_p\sqrt{2\pi}\sigma = I_p\times$ FWHM $\times 1.07$, where I_p is the "peak" flux, this implies that line saturation (*i.e.* $I_p = C$) occurs when EW $\approx$ FWHM. The intrinsic FWHM of weak lines in these late-type giants is typically only a few km s^{-1} , *i.e.* lines with EWs of ≈100mÅ and above are saturated. As noted previously, the CaT lines are heavily saturated and typically have EWs well above 1Å .

To a reasonable approximation, the noise in the continuum (σ_n per Å) due to sky plus object dominates, and over any individual line the continuum level/Å , C, can be taken to be constant. Therefore, the EW and its error due to random noise, ΔEW, are given by

$$EW = \frac{\eta}{C} \qquad \Delta EW = \frac{\sigma_n\sqrt{w}}{C} = \frac{\sqrt{w}}{s:n} \tag{1}$$

where the total line flux is η, $s:n$ is the signal-to-noise per Å and w is the effective width (Å) the line is integrated over.

For a fitted Gaussian profile

$$w = \sqrt{4\pi}\sigma \approx 1.5\ FWHM \tag{2}$$

hence

$$\Delta EW = \frac{\sqrt{1.5\ FWHM}}{s:n} \tag{3}$$

and the FWHM of the line and continuum signal-to-noise are the primary abundance error drivers from a random noise point-of-view. For example, the the two strongest CaT lines, $\lambda_{8542\mathring{A}}$, $\lambda_{8662\mathring{A}}$, used in our analysis have FWHM at a resolution of R=6500 of 2Å –3Å , which for a continuum signal-to-noise of 10/Å implies a lower bound on the combined EW error of ≈0.3Å .

In a similar way we can place constraints on the accuracy of measuring velocities. For Gaussian-like line profiles, which is a good approximation even for native saturated lines like the CaII NIR triplet, the minimum variance bound on the error in the estimated line position $\hat{\lambda}$ is given by

$$var\{\hat{\lambda}\} = \frac{\sigma^2}{\eta}\ \frac{\sigma_n^2\sqrt{16\pi}\ \sigma}{\eta} \tag{4}$$

where the line flux is η and where the noise in the continuum, σ_n $(/\mathring{A})$, dominates and can be taken to be a constant over the region of interest. Rewriting this in terms of the FWHM of the line, the EW and the continuum signal-to-noise, leads to

$$\Delta\hat{\lambda} \approx \frac{FWHM^{\frac{3}{2}}}{EW\ s:n} \tag{5}$$

where again all measurements are per Å.

As an example, for observations at R=6500, the FWHM of the strongest CaT line is typically between 2–3Å , while the EW of these lines is typically ≈2Å ,implying accuracies of wavelength centering at a continuum signal-to-noise of 10/Å of around 0.2Åper line, or equivalently ≈5 km/s using all threee CaT lines. This is the minimum signal-to-noise we consider acceptable in our analysis and is achievable on VLT FLAMES for V=20 objects in 3600s of integration.

2.4 HR analysis

.... the salient features ....

It would be good to put a brief description here ....
....

END-OF-MIKE's bit

2.5 Somethingorother

As noted earlier we ....

we derived the velocities of our sample in two different ways: 1. through cross-correlation of every spectrum with a template consisting of 3 Gaussians with the correct relative amplitude expected for the CaII triplet lines ($V_{\rm CC}$); 2. fitting Gaussians to the individual CaII triplet lines. From the latter, we derive for each line a velocity, V_i and its error σ_i. The velocity from Gaussian fitting ($V_{\rm GAU}$) is then the weighted mean of the 3 CaT velocities ($V_{\rm GAU} = \Sigma \frac{w_i\,V_i}{w_i}$, where the weight $w_i = 1/\sigma_i^2$); the error in $V_{\rm GAU}$ is the inverse of the sum of the weights. As a sanity check, we calculate the difference between $V_{\rm CC}$ and $V_{\rm GAU}$ and assume as error in velocity the largest of half of the difference and the error in the weighted mean. The typical error in velocity was found to be $\lesssim 2$ km s^{-1} .

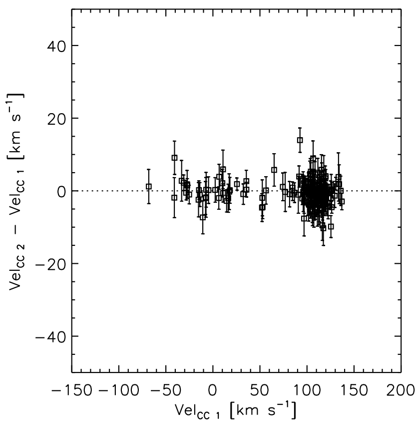

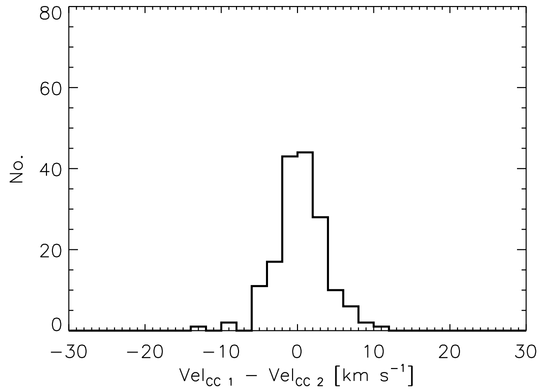

Figure 3. Comparison between velocity measurements for stars with multiple observations, a S/N> 10 and error in velocity < 5 km s^{-1} .

2.5.1 *Old observations*

Out of a total of 1166 targets, 402 have double and 59 triple measurements (from 705 individual targets). Two different set-ups (i.e. different fibres) were used to observe 6 of the 10 fields, with the aim of testing the reliability of the derived velocities and the stability of the instrument. Figure 3 shows the comparison between the velocities from cross-correlation derived for the stars with repeated measurements, S/N per pixel larger than 10 and error in velocity < 5 km s^{-1} (165 objects). The quality of the comparison improves considerably if we exclude the targets with S/N < 10 and error in velocity > 5 km s^{-1} ; 4 objects out to 165 have velocities that do not agree within 2σ (88 out to 402 if we do not put any constraint, i.e. 1/4 of the stars with double measurements). Thus, to make sure the spectra are of adequate quality, we use only the stars with S/N per pixel larger than 10 and error in velocity < 5 km s^{-1} .

2.5.2 *Nov 2005 observations*

Between the 6-8 November 2005, VLT/FLAMES data were acquired for other 5 fields in quite poor weather conditions. Two of these fields were observed twice with the same set-up (same plate and same fibre configuration). For stars with S/N per pixel larger than 10 and error in velocity < 5 km s^{-1} , the average difference in the derived velocities are of the order of 1 km s^{-1} , with r.m.s. of $\sim$ 3.5 km s^{-1} ; the EW for the 3 CaT lines agree remarkably well, with average difference $\sim$ 0.1 Åand largest r.m.s., 0.35 Å, given by the 3rd CaT line.

2.5.3 *Comparison between old and Nov 2005 observations*

Before combining the dataa presented in in Tolstoy et al. (2004) and the data acquired in Nov 2005 we clean our sample from broken fibres and spectra not consistent with what expected for an RGB stars. We removed 7 stars because inadvertly assigned to fibres unavailable at the time of the observations and 7 objects because their spectra was not compatible with an RGB spectrum.

Among the stars in this cleaned-up list there are 87 overlapping stars between the old data-set and the data acquired in Nov 2005 (S/N per pixel larger than 10 and error in velocity < 5 km s^{-1}). The velocity measured in Nov 2005 are in average sistematically higher with respect to the older velocities, of 1.8 km s^{-1} . We thus apply this empirical shift to our sample. Of these, just 7 have a difference in velocity larger than 2σ. Excluding these stars, the average difference in velocity is

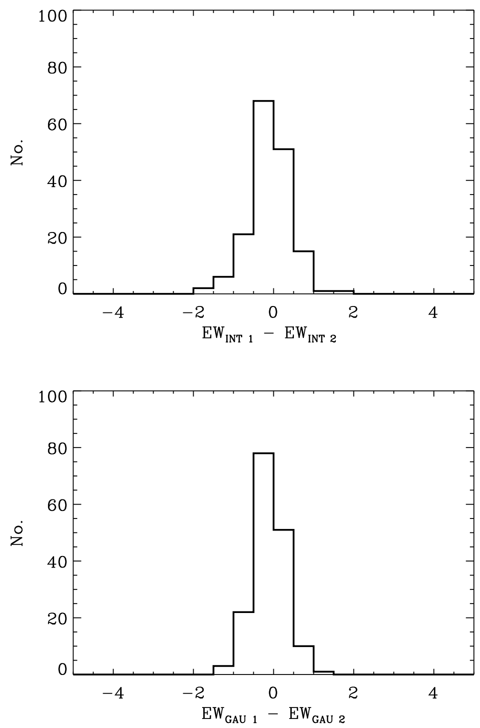

Figure 4. Comparison between EW measurements for stars with multiple observations, a S/N> 10 and error in velocity < 5 km s^{-1} (left: flux integration; right: Gaussian fitting).

2.5.4 All

The final sample was carefully selected to weed out any spurious objects (e.g. broken fibres, background galaxies, foreground stars, etc.). We removed 4 objects due to broken fibres; found no background galaxies and removed 4 objects because spectra are not consistent with RGB stars. Following the S/N and velocity error criteria we rejected 262 stars out of the remaining 698 spectra. Our final sample thus consists of 436 stars.

After deriving the velocities, we obtained the CaII triplet equivalent widths, again using two methods: 1. summing the line flux within a window of 15 Å centred on each CaII triplet line positions (found by the above Gaussian fit); 2. fitting Gaussians to the individual lines.

We found that the best estimate is given by the Gaussian EWs. The comparison between CaT equivalent widths from the two methods for the stars with multiple measurements and S/N > 10 is shown in Fig. 4 (left: method 1; right: method 2). The standard deviation of the two distributions are 0.49 and 0.38 Å; this corresponds, respectively, to an error of $\sim$ 0.2 and 0.15 dex in metallicity, typical for intermediate resolution spectroscopy.

3 CAT CALIBRATION

The next step is to convert the CaT EWs measurements into [Fe/H]. The dependence of CaT EWs strength on metallicity is theoretically difficult to understand, however empirically proved by extensive work in the literature (Armandroff & Zinn, 1988; Diaz et al. 1989; Armandroff & Da Costa 1992; Rutledge et al. 1997.....). Armandroff & Zinn (1988), using integrated light from globular clusters, found that metallicity is the main parameter that governs the EW of the CaT. Diaz et al. (1989) examined a sample of 106 late type stars and found that 97% of the variance in the CaT strenght, defined as a combination of the EW of the individual CaT lines, is due to a linear combination of *logg* and [Fe/H]. The strength of the feature increases with increasing metallicity and decreasing gravity. No strong dependence on $T_{\rm eff}$ was found. The effect of gravity is theoretically understood: as explained in Jorgensen et al. (1992), the line strength of the dominant ionisation stage of an element increases as pressure decreases (*logg*) when the H^- dominates the stellar opacity, and in RGB stars CaII is the dominant ionisation stage.

In order to remove the effect of gravity on the CaT strength, a "reduced equivalent width" is derived:

$$W' = \Sigma W + \beta \times (V - V_{\rm HB}) \tag{6}$$

where $V_{\rm HB}$ is the mean magnitude of the horizontal branch and ΣW is the line strength index, a linear combination of the CaII triplet EWs. Thus, this relation takes into account the fact that at fixed metallicity RGB stars with the same V magnitude will have the same ΣW, whilst the more luminous the RGB, the larger the ΣW. Stars belonging to a globular cluster will fall on a straight line in the ΣW, $V - V_{\rm HB}$ plane. Using $V_{\rm HB}$ removes any strong dependence from the distance or/and reddening. With the above definition, the value of W′ is directly correlated with the metallicity.

To discuss 1) How well V-VHB traces logg; 2) determining VHB for composite stellar populations.

The most extensive calibration of the CaT has been carried out by Rutledge et al. (1997); using 52 globular clusters they found $\beta = 0.64 \pm 0.02$Åmag^{-1} across the range $-2.1 <$ [Fe/H] < -0.6. Cole et al. (2004) re-determined the value of β for their sample, which included globular and open clusters. They found $\beta = 0.66 \pm 0.03$Åmag^{-1} when using only globular clusters, similar to the value found by Rutledge et al. (1997), and $\beta = 0.73 \pm 0.03$Åmag^{-1} when including also the open clusters.

The first uncertainty in using the CaT calibration is of course which combination of the 3 CaII lines should be used. In the literature there are several examples: Rutledge et al. 1997 (hereafter R97) found that the best results are given by a weighted sum of the 3 lines; Tolstoy et al. 2001 (T01) exclude the first CaT line from the sum; Cole et al. 2004 (C04) use an unweighted sum of the 3 lines. Such a choice usually depends on the quality of the data-set: in case of limited signal-to-noise, the weakest line of the CaT is often contaminated by sky-lines and so the determination of its EW is not always reliable.

All these works calibrated the CaT reduced equivalent width on the Carretta & Gratton scale 1997, meaning that the relation between [Fe/H] and W′ has been derived assuming that the calibration clusters have the metallicities derived by Carretta&Gratton 1997 (hereafter CG97). To define their [Fe/H] scale, CG97 re-analysed high-quality EWs from different sources, using a homogeneous compilation of stellar atmosphere parameters, *gf* values and so on, making the largest and most self-consistent analysis of this kind. It is important to note that even the high resolution values of the metallicity for globular clusters can differ significantly from each other (see Pritzl et al. 2005). Obviously, choosing a different metallicity scale implies that the derived relations will be different.

This variety of approaches and calibrations can lead to some kind of confusion when viewing the literature. It is not possible to find out a priori which way of summing CaT EWs and which calibration must be used; we thus test each of the mentioned approaches from the literature and see which one performs better for our data-set.

We use VLT/FLAMES data for a sample of 4 globular clusters: NGC104, NGC5904, NGC3201, NGC4590. The data for NGC104 were taken during an observing run in January 2005, whilst the other ones are from ESO archive. The photometry and astrometry come from Stetson[2]. We reduced all the data using the GIRAFFE pipeline and our own software to derive the velocities and the EWs, in the same way we reduced Scl and Fnx data.

We derive the systemic velocity and velocity dispersion of each cluster following an iterative procedure. The results are summarized in Table 1. We assign membership to those stars with velocity within 3σ from the systemic velocity. For the analysis, we select only stars on the RGB, with V-VHB < 0, S/N$>$ 10 and error in velocity < 5 km s^{-1} .

Fig. 5 shows ΣW versus (V-$V_{\rm HB}$) for the 4 GCs , summing the CaT lines as in R97, T01, C04 (from top to bottom, respectively). The lines represent the relation between Σ W and (V-$V_{\rm HB}$) derived in the above papers using the metallicity scale published by CG97 or fitting the metallicity (dotted and soled, respectively; see Tab. 1 for best-fitting metallicity values). In Fig. 6 we show the best-fitting reduced equivalent widths for the 4 GCs against their metallicity on the CG97 scale. The dotted lines show the [Fe/H] versus W$'$ relation as derived in previous works and the solid lines are the best-fit to the points. We can see different behaviours: the best performance is given by the Tolstoy calibration. The best-fitting [Fe/H] versus W$'$ relation in this case is

$$[\mathrm{Fe/H}]_{\rm CG97} = -2.85 + 0.45W' \tag{7}$$

This means that a star with measured $W' \sim 2$ Åwill be 0.15 dex more metal poor than using the Tolstoy et al. (2001) relation.

Compared to the Tolstoy relation, the Rutledge relation streches the metallicity distribution such that the metallicity is lower at the small W$'$ and higher for large W$'$. The Cole relation produced a small sistematic shift ($\sim$ 0.1-0.15 dex. However, the globular clusters data have a much higher signal-to-noise ratio than our LR data for Scl and Fnx, thus the use of the first CaT line would introduce more noise in our metallicity determination. Given the better performance of the T01 method on our GC dataset, hereafter we will exclude the first CaT line and use the following equations when comparing LR and HR metallicities.

$$W' = (W_2 + W_3) + 0.64 \times (V - V_{\rm HB}) \tag{8}$$

$$[\mathrm{Fe/H}] = -2.85 + 0.45W' \tag{9}$$

$$[\mathrm{Fe/H}] = -2.66 + 0.42W' \tag{10}$$

[2] http://cadcwww.hia.nrc.ca/cadcbin/wdb/astrocat/stetson/query

4 COMPARISON TO HIGH RESOLUTION [FE/H] MEASUREMENTS

Another uncertainty is if these relations, calibrated on globular clusters, can be applied to field stars in galaxies, for example in dSphs. Some dSphs contain intermediate age and even young stellar populations and have a large spread in metallicity, whilst the above relations have been derived for single age stellar population older than 10 Gyr and for a narrower metallicity range. Furthermore, in composite populations it is more difficult to assign a unique magnitude for the horizontal branch. Although Cole et al. (2000, 2004) show that the uncertainty due to this effect in the derived metallicity is not significant.

The only way to reliably test if we can apply the standard GC calibration to field stars is to compare the metallicity derived from CaT EWs to the metallicity obtained from direct measurements of Fe in high resolution (HR) observations of field stars. HR metallicities are more accurate than CaT measurements because the iron abundance is not inferred from other elements but obtained by direct measurement of typically more than 60 separate Fe lines with different ionisation state (i.e. FeI and FeII). HR spectroscopy also allows determination of *logg* and $T_{\rm eff}$, and thus to verify in several different ways if the derived stellar parameters result in physically consistent models.

Until now a comparison between HR and LR [Fe/H] has not been carefully done for field stars, partly due to the lack of a large sample. Thanks to instruments like FLAMES, it is now possible to get suitable comparison spectra for many objects at the same time.

As part of the DART Large Program at ESO, HR FLAMES spectra have been taken for 89 probable Scl velocity member stars in the central regions of Sculptor dSph (Hill et al. 2005, in preparation) overlapping to the DART Scl LR data (Tolstoy et al. 2004). For Fnx out of $\sim$ 80 stars in the central region which have HR FLAMES measurements (Letarte et al. 2006), 35 overlap to our LR sample (Battaglia et al. 2006). Figure 7 shows the comparison between HR and CaT metallicities from our globular cluster calibration. The two methods are in good agreement. The average difference between $[\mathrm{Fe/H}]_{\rm LR}$ and $[\mathrm{Fe/H}]_{\rm HR}$ is -0.05, with scatter 0.16, very similar to the average error in $[\mathrm{Fe/H}]_{\rm HR}$. A slight trend with metallicity seems to be present, with the LR metallicity overestimated of $\sim$ 0.1 dex at the low metallicity end, and underestimated of the same amount at the high metallicity end. We can thus apply the globular cluster calibration to field stars with confidence, at least out to [Fe/H]~ -0.7 dex, where the relation between HR and LR data is linear. It is unclear if the comparison at [Fe/H]> -0.7 dex is indicating a non-linearity in the relationship.

Fig. 8 shows the comparison between CaT metallicities derived from the Tolstoy calibration (Eqs. (2) and (4)), which we used in Tolstoy et al. (2004) and in Battaglia et al.(2006). The trend with metallicity is similar to the previous case, because of the similar slopes in the [Fe/H] versus W$'$ relations (see Eqs.(3) and (4)) ; however the systematic shifts are more enhanced, as in the globular cluster calibration.

we need to understand if this trend with metallicity is due to [Ca/Fe]

Cluster	RA(J2000)	DEC(J2000)	V_{HB}	v_{sys} [km s^{-1}]	$[Fe/H]_{CG97}$	$[Fe/H]_{R97}$	$[Fe/H]_{T01}$	$[Fe/H]_{C04}$
NGC104	$00^h24^m05.2^s$	$-72°04'51''$	14.06	-14.4±0.7	-0.70 ± 0.03	-0.79 ± 0.05	-0.68 ± 0.06	-0.83 ± 0.06
NGC5904	$15^h18^m33.8^s$	$+02°04'58''$	15.07	53.2±0.7	-1.11 ± 0.03	-1.13 ± 0.07	-1.02 ± 0.08	-1.19 ± 0.06
NGC3201	$10^h17^m36.8^s$	$-46°24'40''$	14.77	497.5±1.2	-1.23 ± 0.05	-1.27 ± 0.07	-1.17 ± 0.06	-1.37 ± 0.07
NGC4590	$12^h39^m28.0^s$	$-26°44'34''$	15.68	-98.3±1.7	-1.99 ± 0.06	-1.91 ± 0.06	-1.88 ± 0.07	-2.08 ± 0.06

Table 1. Informations for the globular clusters used in this work. Positions and V_{HB} are from Harris (1996). The systemic velocity v_{sys} was derived in this work. $[Fe/H]_{CG97}$ is the value of metallicity from Carretta & Gratton (1997). $[Fe/H]_{R97}$, $[Fe/H]_{T01}$, $[Fe/H]_{C04}$ are the values of the metallicity from this work, using the calibrations from Rutledge et al. (1997), Tolstoy et al. (2001), Cole et al. (2004). The errors in the derived metallicities were obtained from the standard deviation of the values of reduced equivalent width for each globular cluster.

5 CONCLUSIONS

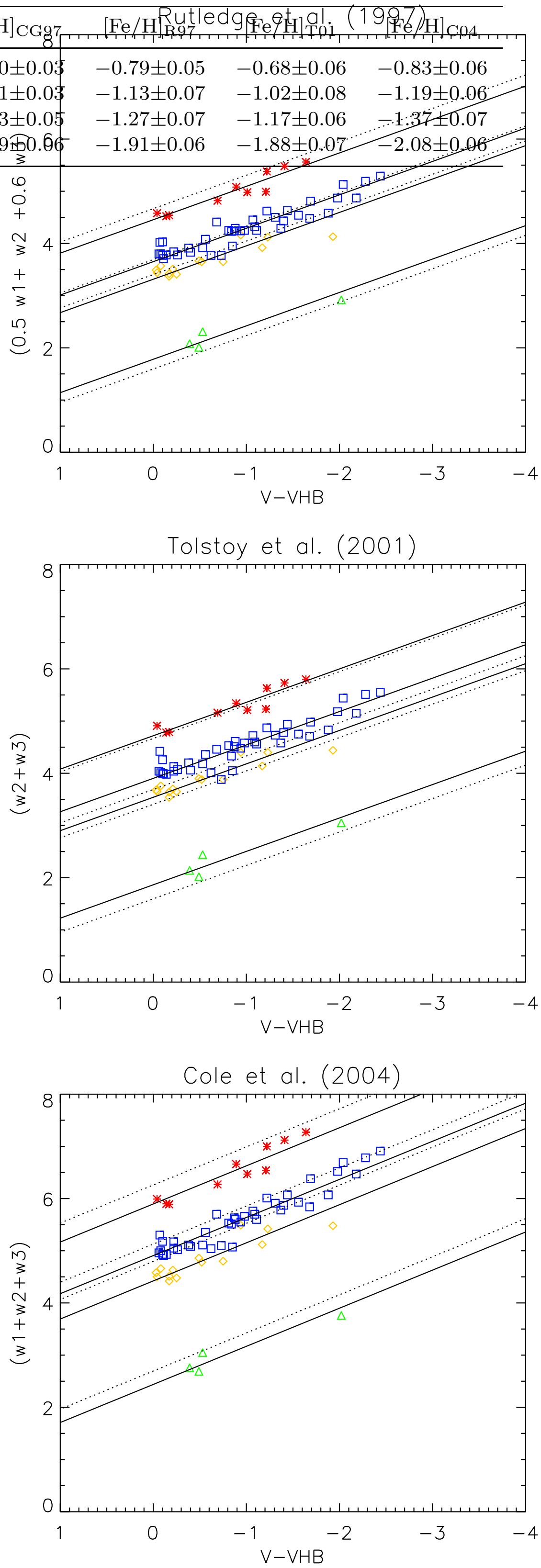

Figure 5. The CaT calibrations: equivalent widths vs. (V-VHB) for RGB stars in 4 globular clusters of different metallicities (asterisks: NGC104; squares: NGC5904; diamonds: NGC3201;triangles: NGC4590), using 3 different linear combinations of CaT lines (from top to bottom: Rutledge, Tolstoy and Cole). The dotted lines show the relations in Rutledge et al. (1997), Tolstoy et al. (2001), Cole et al. (2004), using the metallicity published in CG97; the solid lines show our best-fitting relations. The best-fitting metallicities are summarized in 1.

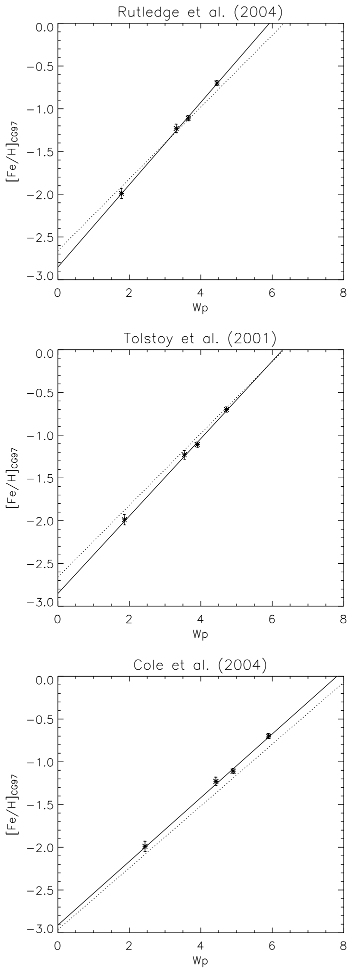

Figure 6. Relation between CG97 metallicity and reduced equivalent width. The reduced equivalent width of each cluster was derived by fitting ΣW .vs. (V-V_{HB}). The solid lines show the best-fitting CG97 metallicity and reduced equivalent width relation for each calibration; the dotted line show the expected CG97 metallicity and reduced equivalent width relation as in the literature. The calibration that represents better the data is the Tolstoy et al.(2001) calibration.

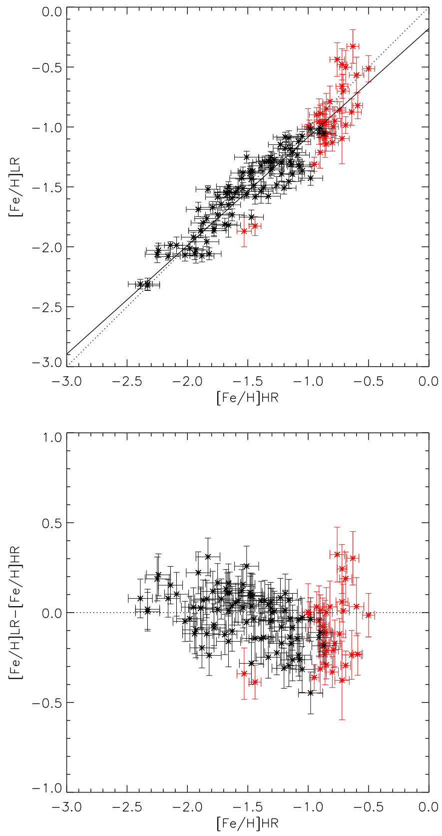

Figure 7. As above, with LR metallicities derived from Eqs. (2) and (3). The average difference between $[Fe/H]_{LR}$ and $[Fe/H]_{HR}$ is −0.05 dex, with a standard deviation of 0.16 dex.

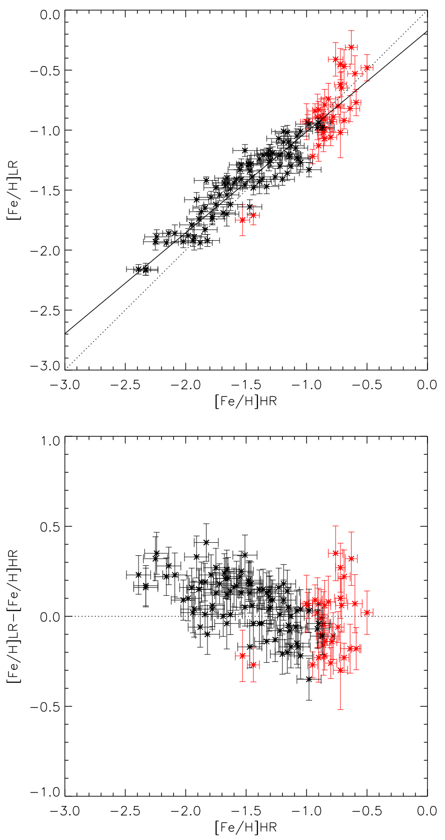

Figure 8. Left: Comparison between metallicities from CaT EWs according to T01 calibration and HR metallicities (Hill et al. 2005) for 89 Sculptor dSph members and 35 Fornax dSph members. Right: Difference between $[Fe/H]_{LR}$ and $[Fe/H]_{HR}$ in function of $[Fe/H]_{HR}$.